Million-fold activation of the [Fe$_2$(μ-O)$_2$] diamond core for C-H bond cleavage

Genqiang Xue[†], **Raymond De Hont**[‡], **Eckard Münck**[‡,*], and **Lawrence Que Jr.**[†,*]

[†]Department of Chemistry and Center for Metals in Biocatalysis, University of Minnesota, 207 Pleasant Street SE, Minneapolis, MN 55455

[‡]Department of Chemistry, Carnegie Mellon University, Pittsburgh, PA 15213

Abstract

In biological systems, the cleavage of strong C–H bonds is often carried out by iron centers – such as the methane monooxygenase in methane hydroxylation – through dioxygen activation mechanisms. High valent species with [Fe$_2$(μ-O)$_2$] diamond cores are thought to act as the oxidizing moieties, but the synthesis of complexes that cleave strong C–H bonds efficiently has remained a challenge. We report here the conversion of a synthetic complex with a valence-delocalized [Fe$^{3.5}$(μ-O)$_2$Fe$^{3.5}$]$^{3+}$ diamond core (**1**) into a complex with a valence-localized [HO-Fe^{III}-O-Fe^{IV}=O]$^{2+}$ open core (**4**), which cleaves C–H bonds over million-fold faster. This activity enhancement results from three factors: the formation of a terminal oxoiron(IV) moiety, the conversion of the low-spin ($S = 1$) Fe^{IV}=O center to a high-spin ($S = 2$) center, and the concentration of the oxidizing capability to the active terminal oxoiron(IV) moiety. This suggests that similar isomerization strategies might be employed by nonheme diiron enzymes.

The controlled oxidation of aliphatic C–H bonds is one of the great challenges in synthetic chemistry and typically requires catalysis by transition metals1. Iron is the most common metal center that Nature employs to oxidize C–H bonds by dioxygen activation mechanisms, in which high-valent oxoiron species are often postulated or demonstrated to act as the actual oxidizing species2–6. These high-valent intermediates cleave C–H bonds through H-atom abstraction mechanisms to generate carbon radicals, which then undergo various transformations such as hydroxylation, halogenation and desaturation. Interestingly, heme enzymes like cytochrome P450 use a low-spin ($S = 1$) oxoiron(IV) center bound to a porphyrin radical as an oxidant7,8, while mononuclear nonheme iron enzymes employ high-spin ($S = 2$) oxoiron(IV) centers6. Furthermore, nonheme diiron enzymes like soluble methane monooxygenase (sMMO) utilize antiferromagnetically coupled high-spin diiron(IV) species to cleave substrate C–H bonds. Based on extended x-ray absorption fine structure (EXAFS) studies, the high-valent oxidant in sMMO called **Q** has been proposed to

have a $[Fe_2(\mu\text{-}O)_2]$ diamond core9, a notion supported by subsequent density functional theory (DFT) calculations10,11. A related diamond core has been deduced for intermediate **X** of the ribonucleotide reductase (RNR) from *E. coli*12 as well as for the corresponding intermediate associated with the RNR from *Chlamydia trachomatis*, which has a MnFe active site13. The variations in nuclearity and spin state among iron oxidants used by Nature to cleave strong C–H bonds raise intriguing questions regarding the relative efficacies of these different strategies. The goal for this study is to gain insight into how structure affects function among these high-valent variants by comparing the relative reactivities of $Fe^{IV}=O$ and $[Fe_2(\mu\text{-}O)_2]$ units in synthetic complexes that are supported by the same tetradentate ligand.

Previously we have characterized model complexes with $[Fe^{III}Fe^{IV}(\mu\text{-}O)_2]^{3+}$ (**1**) and $[Fe^{IV}_2(\mu\text{-}O)_2]^{4+}$ (**2**) diamond cores (Fig. 1) that serve as synthetic precedents for the diamond core structures proposed for intermediates **X** and **Q**14–16. More recently, we have also discovered a diiron(IV) complex, **3**, that has an open $[HO\text{-}Fe^{IV}\text{-}O\text{-}Fe^{IV}=O]^{3+}$ core and converts to **2** upon treatment with one equivalent of strong acid17. Complexes **1** and **2** have been shown to cleave the C–H bond of 9,10-dihydroanthracene (DHA) at −30 °C, oxidizing it to anthracene, but the observed oxidation rates are 2 to 3 orders of magnitude slower than that observed for $[Fe^{IV}(O)(L)(NCMe)]^{2+}$, the corresponding mononuclear oxoiron(IV) complex supported by the same ligand16, suggesting that an oxidant with a terminal Fe=O unit may be more effective for C–H bond cleavage than an oxidant with an Fe-O-Fe unit.

Another important factor that may modulate the reactivity of high-valent iron is the spin state of the iron center18–20. To date, high-valent enzymatic intermediates have been characterized possess low-spin iron(IV) ($S = 1$) centers in heme enzymes7,8 and high-spin iron(IV) ($S = 2$) centers in nonheme iron enzymes4,6. Among the biomimetic iron(IV) complexes characterized thus far, all with porphyrin ligands and almost all with nonheme ligand environments are low spin8,21,22. The few exceptions in the latter subset achieve the high-spin iron(IV) state either by employing an all-aqua ligand set23 or by introducing bulky substituents on the supporting ligand24–26. These large differences in supporting ligand make it difficult to define the factors governing reactivities of high-spin and low-spin complexes. To facilitate reactivity comparisons, we have attempted to find a means to convert an existing low-spin oxoiron(IV) complex into its high-spin analog with only a small change in ligation. In this study, we report the characterization of **4**, a new complex with a high-spin $[HO\text{-}Fe^{III}\text{-}O\text{-}Fe^{IV}=O]^{2+}$ core, which can be generated from either of two previously characterized low-spin diiron complexes, **1** and **3** (Fig. 1); in this report "high-spin" and "low-spin" refer to the spins of the local sites, not the spin of the dinuclear complexes. Complex **4** cleaves the C–H bond of DHA over 10^6-fold faster than **1** and 10^3-fold faster than **3** and $[Fe^{IV}(O)(L)(NCMe)]^{2+}$, thereby demonstrating the much higher reactivity of a high-spin oxoiron(IV) center.

Results and discussion

Generation and characterization of 4

We have previously shown that **3** has an open [HO-Fe^{IV}-O-Fe^{IV}=O]$^{3+}$ core, which converts to the [Fe^{IV}$_2$(μ-O)$_2$]$^{4+}$ diamond core of **2** upon addition of one equivalent of strong acid[17]. If **3** is instead treated with one equivalent of ferrocene at −80 °C, a one-electron reduced species, **4**, is generated that exhibits increased absorption near 450 nm (Fig. 2). This new species is quite unstable and has a lifetime of 60 minutes at −80 °C. It exhibits an isotropic electron paramagnetic resonance (EPR) signal at g = 2.00 that is broadened by the introduction of ^{57}Fe into the complex (Fig. 2, inset), suggesting the generation of an $S = \frac{1}{2}$ iron complex. Quantification of the EPR signal reveals that **4** is produced in ~72% yield with respect to **3**.

Alternatively, **4** can also be obtained by treatment of **1** with 3 equivalents of Bu$_4$NOH at −60 °C. The intense green 600-nm chromophore of **1** decayed concomitant with increased absorption near 450 nm (Fig. S1). Similarly, the characteristic $S = 3/2$ EPR spectrum of **1** was replaced with the isotropic $S = \frac{1}{2}$ signal at g = 2.00 assigned to **4**. At −60 °C, the yield of **4** was only 40% with respect to **1**, presumably due to its much shorter lifetime at −60 °C (complete decay within 10 minutes). Attempts to generate **4** by this method at lower temperature were hampered by problems with incomplete conversion and ice formation from the water present in the Bu$_4$NOH·30H$_2$O solid. The thermal instability of **4** has presented a big challenge to its characterization. Indeed the relatively large fractions of **4** trapped in the experiments described above could be achieved only by the use of the deuterated supporting ligand (Fig. 1), suggesting that ligand oxidation is the limiting factor in these studies.

Taken together, the spectroscopic data obtained thus far, together with the fact that it could be generated by the two distinct methods described above, lead to the hypothesis that **4** possesses an open [HO-Fe^{III}-O-Fe^{IV}=O]$^{2+}$ core structure (Fig. 1). This hypothesis is consistent with the facile one-electron reduction of the [HO-Fe^{IV}-O-Fe^{IV}=O]$^{3+}$ core of **3** as well as the opening of the [Fe^{III}Fe^{IV}(μ-O)$_2$]$^{3+}$ diamond core of **1** by a nucleophilic OH$^-$ (Fig. 1). (While the isomeric [HO-Fe^{IV}-O-Fe^{III}-O$^-$]$^{2+}$ core structure for **4** cannot be ruled out, the demonstrated high basicity of the Fe^{III}-O$^-$ moiety (pK_a ~25)[27] makes this formulation quite unlikely.) A similar core isomerization was proposed for the one-electron oxidation of [Fe^{III}$_2$(μ-O)$_2$(6-Me$_3$-TPA)$_2$]$^{2+}$ (6-Me$_3$-TPA = tris(6-methyl-2-pyridylmethyl)amine) to form an $S = \frac{1}{2}$ Fe^{III}-O-Fe^{IV}=O complex **5**[25]. Indeed **4** and **5** share similar EPR and Mössbauer properties (see below).

We have analyzed the Mössbauer spectra of **4** in considerable depth together with its EPR spectra and described its electronic structure by DFT calculations. The detailed results will be reported in a separate publication, but a small subset of our data is presented here, to demonstrate that the iron sites of **4** are both high-spin and antiferromagnetically coupled. Fig. 3 shows a Mössbauer spectrum of **4** recorded at 4.2 K. The solid line drawn through the data is a fit to an $S = \frac{1}{2}$ spin Hamiltonian. Shown above the data is a decomposition of the spectrum into contributions from a high-spin (S_a =5/2) Fe^{III} (site **a**) and a high-spin (S_b = 2)

Fe^{IV} (site **b**). The spectra shown are quite similar to those reported for **5**, a valence-localized high-spin iron(III)-iron(IV) complex25 and RNR-**X**28,29. For this report the following parameters are relevant. Site **a** has an isomer shift, $\delta = 0.45$ mm s^{-1}, that is typical of high-spin Fe^{III}. The (local) ^{57}Fe magnetic hyperfine coupling is nearly isotropic, with a$_{ave}$= −28.8 MHz, which is typical of high-spin Fe^{III} sites of the present ligand30. Thus, our data unambiguously show that site **a** is high-spin Fe^{III}. Site **b** has $\delta = 0.09$ mm/s, a value indicative of Fe^{IV}, and the components of its a-tensor are all positive. The observation that the a-tensors of the two iron centers are opposite in sign is a strong indication that **4** is an antiferromagnetically coupled dinuclear complex. As site **a** has local spin $S_a = 5/2$ and the spin of the dinuclear cluster is $S = \frac{1}{2}$, the Fe^{IV} site must be high-spin ($S_b = 2$) as well.

We have irradiated a Mössbauer sample of **3** at 77 K with ^{60}Co (5 Mrads over a period of 5 hours), conditions under which only electron transfer can occur and no structural change is possible. The resultant Mössbauer spectrum was indistinguishable from that of **4**, supporting the notion that **3** and **4** share the same core structure but differ in the oxidation and spin state of the Fe-OH moiety. It is interesting to note that the Fe^{IV}=O moiety of **4** has $S_b = 2$ while that of **3** has $S_b = 1$. Thus, unlike the previously reported high-spin oxoiron(IV) complexes that require substantial ligand modifications from their low-spin analogs, **3** and **4** represent a pair of high-spin/low-spin complexes with closely related structures.

Substrate oxidation

The successful generation of **4**, a complex with a [HO-Fe^{III}-O-Fe^{IV}=O]$^{2+}$ core with individual high-spin iron sites, adds a key component previously missing in a series of oxoiron(IV) complexes supported by the same tetradentate ligand (Fig. 1). This series, including mononuclear [Fe^{IV}(O)(L)(NCMe)]$^{2+}$, now consists of five complexes differing in core structure, oxidation state, or spin state that allow us to probe how these factors might affect the rates of C–H bond cleavage and oxygen atom transfer by the oxoiron(IV) unit. Unless otherwise stated, all kinetic measurements were performed under the same conditions for direct comparison of reaction rates (in 3:1 CH$_2$Cl$_2$-MeCN at −80 °C under Ar). The −80 °C temperature used was dictated by the low thermal stability of **4**. Even at this very low temperature, **4** exhibited significant oxidizing power.

As illustrated in Fig. 5, all five complexes of the series can transfer an oxygen atom to diphenyl(pentafluorophenyl)phosphine at −80 °C. The corresponding phosphine oxide was obtained in 65–100% yields (Table 1). Interestingly, diamond-core complexes **1** and **2** reacted at least 10^3-fold slower than the other three complexes with terminal Fe=O units. We speculate that cleavage of the two Fe-O bonds required by oxo transfer from the Fe-O-Fe unit may provide the rationale for their lower reactivity. In contrast, **3**, **4** and [Fe^{IV}(O)(L)(NCMe)]$^{2+}$ were much more reactive and oxidized the phosphine at comparable rates. Thus having a terminal oxo group is the key to efficient oxo transfer, but whether the iron(IV) center is high-spin or low-spin is not important.

The story is quite different for H-atom abstraction by this series of complexes. Addition of DHA (C–H bond dissociation energy (D$_{C–H}$) = 78 kcal mol^{-1})31 to **4** caused decay of its 450 nm chromophore and the concurrent formation of new features at 377 nm and 357 nm

characteristic of anthracene (Fig. 4). Analysis of the reaction solution revealed that anthracene was formed exclusively and in 40% yield with respect to **4**. The oxidation was first-order in both **4** (Fig. 4, inset) or DHA (Fig. S4), with a second order rate constant (k_2) of 28 M^{-1} s^{-1} at –80 °C (Table 1). A large deuterium kinetic isotope effect (D-KIE) of 50 was obtained when DHA-d_4 was used as substrate, showing that the oxidation by **4** involves rate determining C–H bond cleavage. Furthermore the very large D-KIE suggests that C–H bond cleavage occurs with a significant tunneling component. This value is larger than that found for DHA oxidation (18 at –30 °C) by the recently characterized high-spin oxoiron(IV) complex of a sterically bulky tripodal ligand26 but comparable to that observed for the high-spin oxoiron(IV) intermediate of the 2-oxoglutarate-dependent enzyme TauD reported by Bollinger and Krebs for the hydroxylation of the substrate taurine (~50 at 25 °C)32.

Fig. 5 compares the relative reactivities of the various oxoiron(IV) complexes in this study and Table 1 provides the second order rate constants measured; additional experimental data can be found in SI (Figs. S3 to S7). From these data, it is clear that the open-core high-spin $Fe^{III}Fe^{IV}$ complex **4** is the most reactive of the series, oxidizing DHA over a million-fold faster than **1**, its low-spin $Fe^{III}Fe^{IV}$ precursor with an $[Fe_2(\mu\text{-}O)_2]$ diamond core. This rate enhancement corresponds to a decrease in activation energy by greater than 5.4 kcal mol^{-1} (based on $E_a = -RT \ln k_2$), suggesting that coordination of a hydroxide ligand to the $[Fe_2(\mu\text{-}O)_2]$ diamond core of **1** provides a means of unleashing its oxidizing potential. The following pairwise comparisons provide further insights into what factors affect the reactivities of these oxoiron(IV) complexes.

The first comparison is between the two diiron(IV) complexes, **2** with an $[Fe^{IV}_2(\mu\text{-}O)_2]^{4+}$ diamond core versus **3** with an $[OH\text{-}Fe^{IV}\text{-}O\text{-}Fe^{IV}=O]^{3+}$ open core, both of which have low-spin iron(IV) centers17,33. Under the same conditions, **3** was found to oxidize DHA 100-fold faster than **2** (Table 1). For **2**, hydrogen-atom abstraction must involve one of the oxo bridges of its $[Fe^{IV}_2(\mu\text{-}O)_2]^{4+}$ diamond core to form an initial hydroxo-bridged $Fe^{III}Fe^{IV}$ product, which could be readily deprotonated by 2,6-lutidine to generate **1**16. On the other hand, C–H bond cleavage by **3** must involve its terminal oxoiron(IV) unit and occurs at a rate comparable to that observed for mononuclear $[Fe^{IV}(O)(L)(NCMe)]^{2+}$ (Table 1). Therefore, the higher reactivity of **3** compared to **2** suggests that a terminal oxo is more reactive than a bridging oxo for H-atom abstraction. This reactivity difference may be attributed to the higher unpaired spin density on the oxo group of a terminal oxoiron(IV) moiety20.

The second comparison is between **3** and **4**, two complexes that share the same open [HO-Fe-O-Fe=O] core but differ in the oxidation state of the Fe-OH unit and, perhaps more importantly, the spin states of the iron centers. Although **4** has an $Fe^{III}\text{-}O\text{-}Fe^{IV}$ unit, it is a thousand-fold more reactive than **3** with the more oxidized $Fe^{IV}\text{-}O\text{-}Fe^{IV}$ unit. We attribute the much higher reactivity of **4** to the high-spin nature ($S = 2$) of its oxoiron(IV) moiety. This comparison provides the first convincing experimental evidence for the DFT-derived consensus that the $S = 2$ manifold is kinetically more reactive than the corresponding $S = 1$ state18–20,34,35. DFT calculations have suggested that the unoccupied frontier molecular orbitals (FMOs) contribute to the reactivity difference of high-spin/low-spin complexes20,35, because the high-spin oxoiron(IV) unit has an additional reaction channel

involving the σ-FMO pathway[20]. Given that there are only a few spectroscopic results thus far on synthetic high-spin oxoiron(IV) complexes[23–26], ongoing spectroscopic comparisons of **3** and **4** coupled with DFT calculations should provide more insights into how electronic structure affects the reactivity of high-spin oxoiron(IV) species.

The open-core complexes **3** and **4** can be compared with some available data for oxoiron(IV) porphyrin cation radical complexes. At −40 °C, **3** oxidized DHA with a k_2 of 5.5 M^{-1} s^{-1} in MeCN , comparable to the k_2 of 6.6 M^{-1} s^{-1} for [Fe^{IV}(O)(TMP)]$^+$ (TMP = 5,10,15,20-tetramesitylporphinate) in 1:1 CH_2Cl_2/MeCN[36]. These values obtained at −40 °C are a factor of 4–5 smaller than that measured for **4** in 3:1 CH_2Cl_2/MeCN at −80 °C, which emphasizes the much greater reactivity of the high-spin complex. A much more reactive heme model complex, [Fe^{IV}(O)(TMPyP)]$^+$ (TMPyP = 5,10,15,20-tetrakis(*N*-methyl-4'-pyridyl)porphinate), was recently observed by stopped flow methods, demonstrating the effect porphyrin substituents can have in enhancing the reactivity of the Fe^{IV}=O unit. [Fe^{IV}(O)(TMPyP)]$^+$ oxidized xanthene ($D_{C–H}$ = 75 kcal mol^{-1})[31] with a k_2 of 3.6×10^6 M^{-1} s^{-1} in aqueous media at pH 4.7 and 14.5 °C [37]. From the plot shown in Fig. 3 of ref. 37, a tenfold smaller k_2 value for DHA oxidation can be estimated, so [Fe^{IV}(O)(TMPyP)]$^+$ at 14.5 °C is 10^4 more reactive than **4** at −80 °C. Given the nearly 100° temperature difference, it is conceivable that **4** may in fact approach [Fe^{IV}(O)(TMPyP)]$^+$ in oxidizing power, so a nonheme Fe^{IV}=O in a high-spin state could exhibit comparable C–H bond cleaving reactivity as a low-spin Fe^{IV}=O bound to a porphyrin cation radical. Stopped flow experiments are planned to characterize the reactivity of **4** at higher temperatures as well as those of its more reactive analogs.

Both **3** and **4** can also oxidize substrates with C–H bonds having $D_{C–H}$ greater than that of DHA (78 kcal mol^{-1}). Tetrahydrofuran (THF) with a $D_{C–H}$ of 93 kcal mol^{-1} (31) was oxidized by **3** at 10 °C to γ-butyrolactone in 38% yield with a k_2 of 0.43 M^{-1} s^{-1}. A D-KIE value of 15 (Fig. S8) was obtained for this reaction, indicating rate determining C–H bond cleavage. For comparison, the THF oxidation rate of **3** was 3-fold faster than that of a recently reported (μ-oxo)diiron(IV) complex **6**[38], which exhibited a k_2 of 0.13 M^{-1} s^{-1} under the same reaction conditions. Complex **6** has an Fe^{IV}Fe^{IV}/Fe^{III}Fe^{IV} redox potential of 1500 mV vs. ferrocene/ferrocenium (Fc$^{+/0}$), which is at least 0.8 V higher than that for **3** (between 490 and 670 mV). The observation that **3** and **6** have comparable THF oxidation rates despite a much greater thermodynamic driving force for the latter is another piece of evidence to support the notion that a terminal Fe^{IV}=O unit like that found in **3** is significantly more reactive towards C–H bonds than the Fe^{IV}-O-Fe^{IV} units found in **2** and **6**. However **3** was stable in the presence of THF at −80 °C. In contrast, **4** was still able to oxidize THF to γ-butyrolactone in 23% yield with a k_2 of 0.03 M^{-1} s^{-1} and a D-KIE of 45 (Fig. S9). This result provides further corroboration for the much higher reactivity of the high-spin complex **4** compared to its low-spin structural counterpart **3**.

We emphasize that the C–H bond cleavage reactivities reported here are based on kinetic measurements that can be related to the intrinsic hydrogen-atom affinity of a metal-oxo reagent. This affinity is a thermodynamic factor equivalent to the D_{O-H} of the newly formed Fe^{III}O-H bond[39]. According to a thermodynamic cycle developed by Bordwell[40] and applied to metal-oxo systems by Mayer[41], this bond strength depends on the one-electron

reduction potential (E_r) of the M=O unit and the pK_a of the M-OH reduction product. Table 1 lists E_r values (vs. ferrocenium/ferrocene (Fc$^{+/0}$)) of the high-valent complexes studied here. Only the E_r for **2** of 760 mV could be established by cyclic voltammetry, while the other values had to be estimated from experiments with chemical reductants that allowed us to define a redox potential range. Complex **1** has the lowest E_r of the series, while **3**, **4** and [Fe^{IV}(O)(L)(NCMe)]$^{2+}$ have E_r values between 470 and 670 mV. Although **2** has the highest E_r of the series, it oxidizes DHA 100-fold more slowly than **3** and 10^5-fold more slowly than **4** (Table 1), showing that structural and spin-state features indeed contribute to the significant kinetic differences between these complexes.

The other factor to consider is the pK_a's of corresponding reduced species, none of which is known. However, we argue that the pK_a of an Fe^{III}-OH-Fe$^{III/IV}$ unit should be significantly lower than that of Fe^{III}-OH unit, because of the binding of a second highly Lewis acidic Fe to the OH group. This argument is supported by the observation that the Fe^{III}-OH-Fe^{IV} species generated from H-atom abstraction by **2** can be converted completely to **1** by treatment with 5 equivalents of 2,6-lutidine in MeCN[16]. From this result, we estimate its pK_a to be around 14, comparable to that of lutidinium ion[42]. The pK_a's for the mononuclear Fe^{III}-OH units of **3**, **4** and [Fe^{IV}(O)(L)(NCMe)]$^{2+}$ formed upon H-atom abstraction should be higher. There is only one such pK_a value in the literature, which was reported by Borovik to be 25 for the crystallographically characterized mononuclear Fe^{III}-O$^-$ complex of a sterically bulky tripodal ligand[27]. It would thus appear that it is the higher basicity of the Fe^{III}-O$^-$ unit that enhances the H-atom abstraction observed for **3** and **4**, an idea that has been demonstrated in Mn-oxo chemistry[43,44].

Concluding Remarks

In the current study, we have shown that complexes with [Fe-O-Fe^{IV}=O] open cores are a hundred- to a million-fold more reactive in C–H bond cleavage than their counterparts with [Fe$_2$(μ-O)$_2$] diamond cores. These results suggest that [Fe$_2$(μ-O)$_2$] diamond cores, at least in the low-spin manifold, are kinetically quite poor oxidants. However, the coordination of OH$^-$ to **1** opens up its diamond core and generates the [OH-Fe^{III}-O-Fe^{IV}=O] open core complex **4**, which is over a million-fold more reactive than **1**. The dramatic increase in reactivity towards C–H bonds can be attributed to two main factors: 1) the formation of a terminal oxoiron(IV) moiety, which contributes a thousand-fold enhancement, and 2) the spin-state change of the iron centers from low spin to high spin, which provides another thousand-fold increase. The million-fold difference in reactivity between **1** and **4** may also rationalize the 200-fold enhancement in the DHA oxidation rate of **1** observed upon addition of 1 M water by invoking formation of 0.02% of **4** in the water-binding equilibrium[45]. In contrast, only factor #1 appears to play a role in oxo transfer, as the spin-state change does not elicit any difference in reaction rate among the complexes with terminal Fe=O units.

Complexes **3** and **4** represent the only pair of low-spin/high-spin complexes that share the same supporting ligand and core structure. These structural similarities allow us to unambiguously attribute the thousand-fold higher reactivity of **4** for C–H bond cleavage to the high-spin nature ($S = 2$) of its oxoiron(IV) moiety. The reactivity comparison between **3** and **4** provides the first convincing experimental evidence to support the prevailing DFT-

derived consensus that the $S = 2$ Fe^{IV}=O manifold is kinetically more reactive[18–20,34,35]. Our success in generating **4** also opens a new avenue for further exploring how electronic structure correlates with the reactivity of high-spin oxoiron(IV) species.

The much higher reactivity of **4** towards C–H bonds is also illustrated by the strength of the C–H bonds that can be cleaved. While **1** can barely cleave the C–H bond of DHA ($D_{C-H} = 78$ kcal mol^{-1}) at –80 °C, **4** cleaves the much stronger C–H bond of THF ($D_{C-H} = 93$ kcal mol^{-1}) within minutes under the same conditions. The activation of **1** to **4** involves changes in both core geometry and electronic structure. In the course of core isomerization, valence-*delocalized* **1** converts to valence-*localized* **4**, thereby changing the effective oxidation state of the individual iron centers from +3.5 in **1** to +4 for one iron center in **4** and concentrating the oxidizing power on the Fe=O unit to cleave the target C–H bond. Extension of this notion to the catalytic mechanism of methane monooxygenase raises the possibility for the isomerization of the Fe^{IV}Fe^{IV} diamond core of sMMO intermediate **Q** to an Fe^{III}Fe^{V} form as an excellent strategy to cleave the very strong C–H bond of methane ($D_{C-H} = 104$ kcal mol^{-1})[31] while protecting active site residues that have weaker C–H bonds. This idea has also found support from DFT calculations on the mechanism of sMMO[46,47]. In this mechanistic scenario, only when substrate is bound at the active site would the oxidizing power of **Q** be fully unmasked.

Methods

Physical Methods

UV-vis spectra were recorded on a Hewlett-Packard 8453A diode array spectrometer equipped with a cryostat from Unisoku Scientific Instruments, Osaka, Japan. Mössbauer spectra were recorded with two spectrometers, using Janis Research (Wilmington, MA) SuperVaritemp dewars that allow studies in applied magnetic fields up to 8.0 T in the temperature range from 1.5 to 200 K. Mössbauer spectral simulations were performed by using the WMOSS software package (WEB Research, Minneapolis). Isomer shifts are quoted relative to Fe metal at 298 K. Perpendicular (9.63 GHz) mode X-band EPR spectra were recorded on a Bruker EPP 300 spectrometer equipped with an Oxford ESR 910 liquid helium cryostat and an Oxford temperature controller. The quantification of all signals was relative to a Cu-EDTA spin standard. Software for EPR analysis was provided by Dr. Michael P. Hendrich of Carnegie Mellon University. ^{31}P NMR spectra were recorded on a Varian VXR-300 spectrometer.

Materials and kinetic measurements

The list of chemicals used and the procedures for complex preparations are provided in supplemental information (SI). All kinetic measurements were performed under Ar. The reaction progresses were monitored by decays of the characteristic absorptions of iron complexes with details provided in SI. Typically, the pseudo-first-order rate constants k_{obs} were obtained by fitting the decay time traces and the second-order rate constants k_2 were obtained by fitting the k_{obs} vs. substrate-concentration plots. The reaction solutions were filtered through silica gel columns to remove iron complexes prior to product analyses. Anthracene was quantified by absorbance of the filtrates at 377 nm ($\varepsilon = 7700$ M^{-1}.cm^{-1}).

Gamma-butyrolactone and anthraquinone were quantified by GC with naphthalene was the internal standard. Diphenyl(pentafluorophenyl)phosphine oxide from oxo-atom transfer reactions was quantified by ^{31}P NMR, with the remaining substrate (typically 2 equivalents) as the internal standard.

Supplementary Material

Refer to Web version on PubMed Central for supplementary material.

Acknowledgements

References

1. Christmann M. Selective Oxidation of Aliphatic C–H Bonds in the Synthesis of Complex Molecules. Angew. Chem. 2008; 47:2740–2742. [PubMed: 18348112]

2. Sono M, Roach MP, Coulter ED, Dawson JH. Heme-Containing Oxygenases. Chem. Rev. 1996; 96:2841–2887. [PubMed: 11848843]

3. Wallar BJ, Lipscomb JD. Dioxygen Activation by Enzymes Containing Binuclear Non-Heme Iron Clusters. Chem. Rev. 1996; 96:2625–2658. [PubMed: 11848839]

4. Solomon EI, et al. Geometric and Electronic Structure/Function Correlations in Non-Heme Iron Enzymes. Chem. Rev. 2000; 100:235–349. [PubMed: 11749238]

5. Costas M, Mehn MP, Jensen MP, Que L Jr. Oxygen Activation at Mononuclear Nonheme Iron: Enzymes, Intermediates, and Models. Chem. Rev. 2004; 104:939–986. [PubMed: 14871146]

6. Krebs C, Fujimori DG, Walch CT, Bollinger JM Jr. Non-Heme Fe(IV)–Oxo Intermediates. Acc. Chem. Res. 2007; 40:484–492. [PubMed: 17542550]

7. Fujii H. Electronic structure and reactivity of high-valent oxo iron porphyrins. Coord. Chem. Rev. 2002; 226:51–60.

8. Groves, JT. Cytochrome P450: Structure, Mechanism, and Biochemistry. 3rd ed.. Ortiz de Montellano, PR., editor. Kluwer Academic/Plenum Publishers; 2005. p. 1-43.

9. Shu L, et al. An $Fe^{IV}_2O_2$ Diamond Core Structure for the Key Intermediate **Q** of Methane Monooxygenase. Science. 1997; 275:515–518. [PubMed: 8999792]

10. Siegbahn PEM. Theoretical Model Studies of the Iron Dimer Complex of MMO and RNR. Inorg. Chem. 1999; 38:2880–2889. [PubMed: 11671034]

11. Baik M-H, Newcomb M, Friesner RA, Lippard SJ. Mechanistic Studies on the Hydroxylation of Methane by Methane Monooxygenase. Chem. Rev. 2003; 103:2385–2420. [PubMed: 12797835]

12. Riggs-Gelasco PJ, et al. EXAFS Characterization of the Intermediate X Generated during the Assembly of the *Escherichia coli* Ribonucleotide Reductase R2 Diferric-Tyrosyl Radical Cofactor. J. Am. Chem. Soc. 1998; 120:849–860.

13. Younker JM, et al. Structural Analysis of the Mn(IV)/Fe(III) Cofactor of *Chlamydia trachomatis* Ribonucleotide Reductase by Extended X-ray Absorption Fine Structure Spectroscopy and Density Functional Theory Calculations. J. Am. Chem. Soc. 2008; 130:15022–15027. [PubMed: 18937466]

14. Dong Y, et al. A High-Valent Nonheme Iron Intermediate. Structure and Properties of [Fe$_2$(μ-O)$_2$(5-Me-TPA)$_2$](ClO$_4$)$_3$. J. Am. Chem. Soc. 1995; 117:2778–2792.

15. Hsu H-F, Dong Y, Shu L, Young VG Jr, Que L Jr. Crystal Structure of a Synthetic High-Valent Complex with an Fe$_2$(μ-O)$_2$ Diamond Core. Implications for the Core Structures of Methane Monooxygenase Intermediate Q and Ribonucleotide Reductase Intermediate X. J. Am. Chem. Soc. 1999; 121:5230–5237.

16. Xue G, et al. A Synthetic Precedent for the [Fe$^{IV}_2$(μ-O)$_2$] Diamond Core Proposed for Methane Monooxygenase Intermediate Q. Proc. Natl. Acad. Sci., USA. 2007; 104:20713–20718. [PubMed: 18093922]

17. Xue G, Fiedler AT, Martinho M, Münck E, Que L Jr. Insights into the P-to-Q Conversion in the Catalytic Cycle of Methane Monooxygenase from a Synthetic Model System. Proc. Natl. Acad. Sci., USA. 2008; 105:20615–20620.

18. Kumar D, Hirao H, Que L Jr, Shaik S. Theoretical Investigation of C–H Hydroxylation by (N4Py)Fe^{IV}=O^{2+}: An Oxidant More Powerful than P450? J. Am. Chem. Soc. 2005; 127:8026–8027. [PubMed: 15926822]

19. Hirao H, Kumar D, Que L Jr, Shaik S. Two-State Reactivity in Alkane Hydroxylation by Non-Heme Iron-Oxo Complexes. J. Am. Chem. Soc. 2006; 128:8590–8606. [PubMed: 16802826]

20. Decker A, et al. Spectroscopic and Quantum Chemical Studies on Low-Spin Fe^{IV}=O Complexes: Fe-O Bonding and Its Contributions to Reactivity. J. Am. Chem. Soc. 2007; 129:15983–15996. [PubMed: 18052249]

21. Shan X, Que L Jr. High-Valent Nonheme Iron-Oxo Species in Biomimetic Oxidations. J. Inorg. Biochem. 2006; 100:421–433. [PubMed: 16530841]

22. Que L Jr. The Road to Non-Heme Oxoferryls and Beyond. Acc. Chem. Res. 2007; 40:493–500. [PubMed: 17595051]

23. Pestovsky O, et al. Aqueous Fe^{IV}=O: Spectroscopic Identification and Oxo Group Exchange. Angew. Chem. Int. Ed. 2005; 44:6871–6874.

24. Dong Y, Que L Jr, Kauffmann K, Münck E. An Exchange-Coupled Complex with Localized High-Spin Fe^{IV} and Fe^{III} Sites of Relevance to Cluster X of *Escherichia coli* Ribonucleotide Reductase. J. Am. Chem. Soc. 1995; 117:11377–11378.

25. Zheng H, Yoo SJ, Münck E, Que L Jr. The Flexible Fe$_2$(μ-O)$_2$ Diamond Core: A Terminal Iron(IV)-Oxo Species Generated from the Oxidation of a Bis(μ-oxo)diiron(III) Complex. J. Am. Chem. Soc. 2000; 122:3789–3790.

26. England J, et al. A Synthetic High-Spin Oxoiron(IV) Complex. Generation, Spectroscopic Characterization and Reactivity. Angew. Chem. 2009; 48:3622–3626. [PubMed: 19373820]

27. Gupta R, Borovik AS. Monomeric Mn$^{III/II}$ and Fe$^{III/II}$ Complexes with Terminal Hydroxo and Oxo Ligands: Probing Reactivity via O-H Bond Dissociation Energies. J. Am. Chem. Soc. 2003; 125:13234–13242. [PubMed: 14570499]

28. Ravi N, Bollinger JM Jr, Huynh BH, Edmondson DE, Stubbe J. Mechanism of Assembly of the Tyrosyl Radical-Diiron(III) Cofactor of *E. coli* Ribonucleotide Reductase. 1. Mössbauer Characterization of the Diferric Radical Precursor. J. Am. Chem. Soc. 1994; 116:8007–8014.

29. Sturgeon BE, et al. Reconsideration of X, the Diiron Intermediate Formed During Cofactor Assembly in *E. coli* Ribonucleotide Reductase. J. Am. Chem. Soc. 1996; 118:7551–7557.

30. Münck, E. Physical Methods in Bioinorganic Chemistry. Spectroscopy and Magnetism. Que, L., Jr, editor. University Science Books; 2000. p. 287-319.

31. Luo, Y-R. Comprehensive Handbook of Chemical Bond Energies. CRC Press; 2007.

32. Bollinger JM Jr, Krebs C. Stalking intermediates in oxygen activation by iron enzymes: Motivation and method. J. Inorg. Biochem. 2006; 100:586–605. [PubMed: 16513177]

33. Martinho M, et al. Mössbauer and DFT Study of the Ferromagnetically Coupled Diiron(IV) Precursor to a Complex with an Fe$^{IV}_2$O$_2$ Diamond Core. J. Am. Chem. Soc. 2009; 131:5823–5830. [PubMed: 19338307]

34. Shaik S, Hirao H, Kumar D. Reactivity of High-Valent Iron-Oxo Species in Enzymes and Synthetic Reagents: A Tale of Many States. Acc. Chem. Res. 2007; 40:523–542.

35. Michel C, Baerends EJ. What Singles out the FeO^{2+} Moiety? A Density-Functional Theory Study of the Methane-to-Methanol Reaction Catalyzed by the First Row Transition-Metal Oxide Dications MO(H$_2$O)$_p^{2+}$, M = V-Cu. Inorg. Chem. 2009; 48:3628–3638. [PubMed: 19301854]

36. Han A-R, et al. Direct evidence for an iron(IV)-oxo porphyrin π-cation radical as an active oxidant in catalytic oxygenation reactions. Chem. Comm. 2008; 2008:1076–1078. [PubMed: 18292895]

37. Bell SR, Groves JT. A Highly Reactive P450 Model Compound I. J. Am. Chem. Soc. 2009; 131:9640–9641. [PubMed: 19552441]

38. Wang D, Farquhar ER, Stubna A, Münck E, Que L Jr. A diiron(IV) complex that cleaves strong C–H and O-H bonds. Nature Chem. 2009; 1:145–150. [PubMed: 19885382]

39. Mayer JM. Hydrogen Atom Abstraction by Metal-Oxo Complexes: Understanding the Analogy with Organic Radical Reactions. Acc. Chem. Res. 1998; 31:441–450.

40. Bordwell FG, Cheng J-P, Ji G-Z, Satish AV, Zhang X. Bond Dissociation Energies in DMSO Related to the Gas Phase. J. Am. Chem. Soc. 1991; 113:9790–9795.

41. Gardner KA, Mayer JM. Understanding C–H Bond Oxidations: H˙ and H⁻ Transfer in the Oxidation of Toluene by Permanganate. Science. 1995; 269:1849–1851. [PubMed: 7569922]

42. Augustin-Nowacka D, Chmurzy ski L. A potentiometric study of acid-base equilibria of substituted pyridines in acetonitrile. Anal. Chim. Acta. 1999; 381:215–220.

43. Yin G, et al. Oxidative Reactivity Difference among the Metal Oxo and Metal Hydroxo Moieties: pH Dependent Hydrogen Abstraction by a Manganese(IV) Complex Having Two Hydroxide Ligands. J. Am. Chem. Soc. 2008; 130:16245–16253. [PubMed: 18998682]

44. Parsell TH, Yang M-Y, Borovik AS. C–H Bond Cleavage with Reductants: Re-Investigating the Reactivity of Monomeric $Mn^{III/IV}$-Oxo Complexes and the Role of Oxo Ligand Basicity. J. Am. Chem. Soc. 2009; 131:2762–2763. [PubMed: 19196005]

45. Johansson AJ, Noack H, Siegbahn PEM, Xue G, Que L Jr. Observed Enhancement of the Catalytic Activity of a Biomimetic Diiron Complex by the Addition of Water - Mechanistic Insights from Theoretical Modeling. Dalton Trans. 2009:4741–4750. [PubMed: 19513484]

46. Siegbahn PEM, Crabtree RH. Mechanism of C–H Activation by Diiron Methane Monooxygenases: Quantum Chemical Studies. J. Am. Chem. Soc. 1997; 119:3103–3113.

47. Rinaldo D, Philipp DM, Lippard SJ, Friesner RA. Intermediates in Dioxygen Activation by Methane Monooxygenase: A QM/MM Study. J. Am. Chem. Soc. 2007; 129:3135–3147. [PubMed: 17326634]
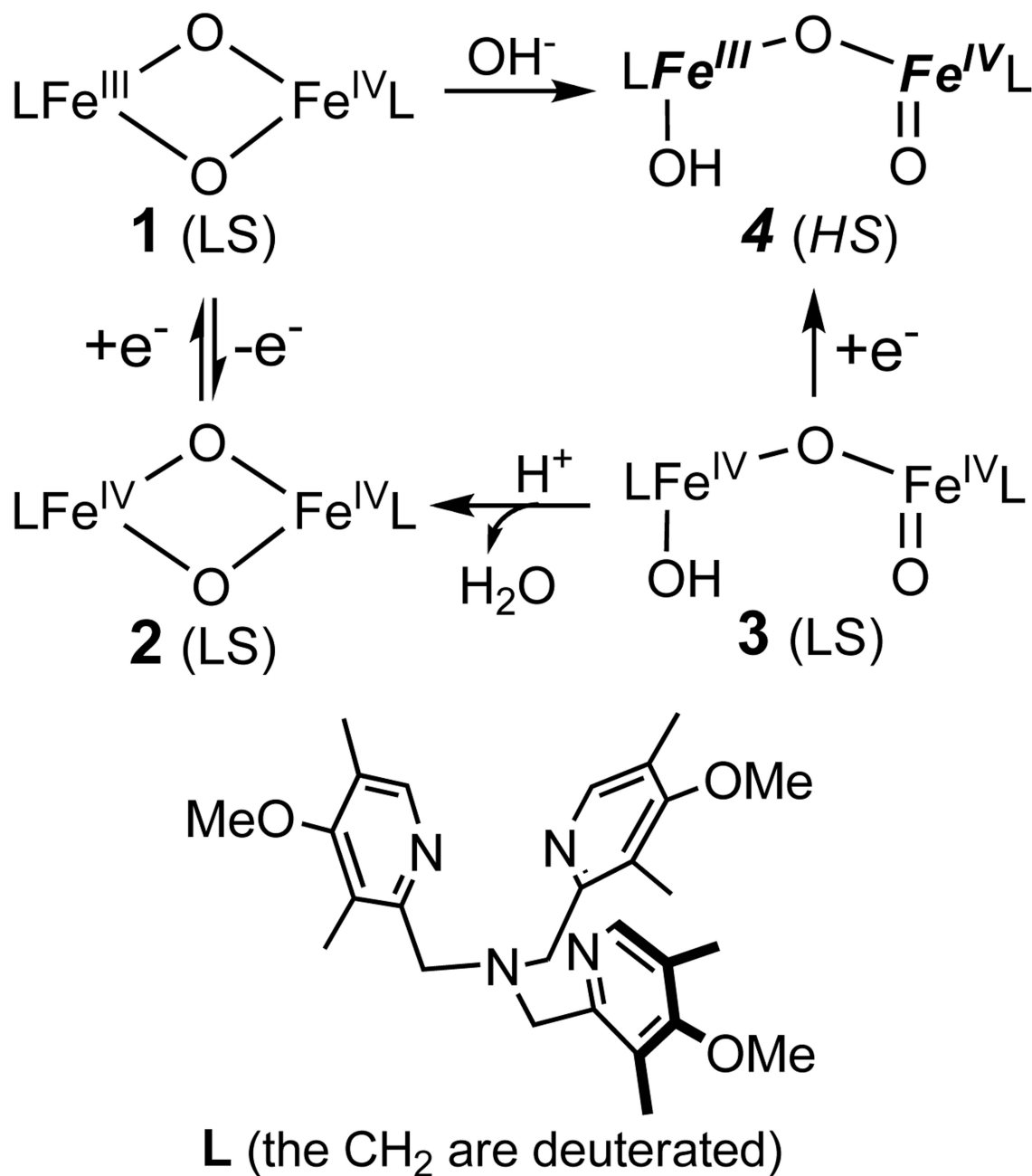
Figure 1.
Interconversions among high-valent diiron complexes in this study. HS (high-spin) and LS (low-spin) refer to the spin states of the individual iron center in each complex.
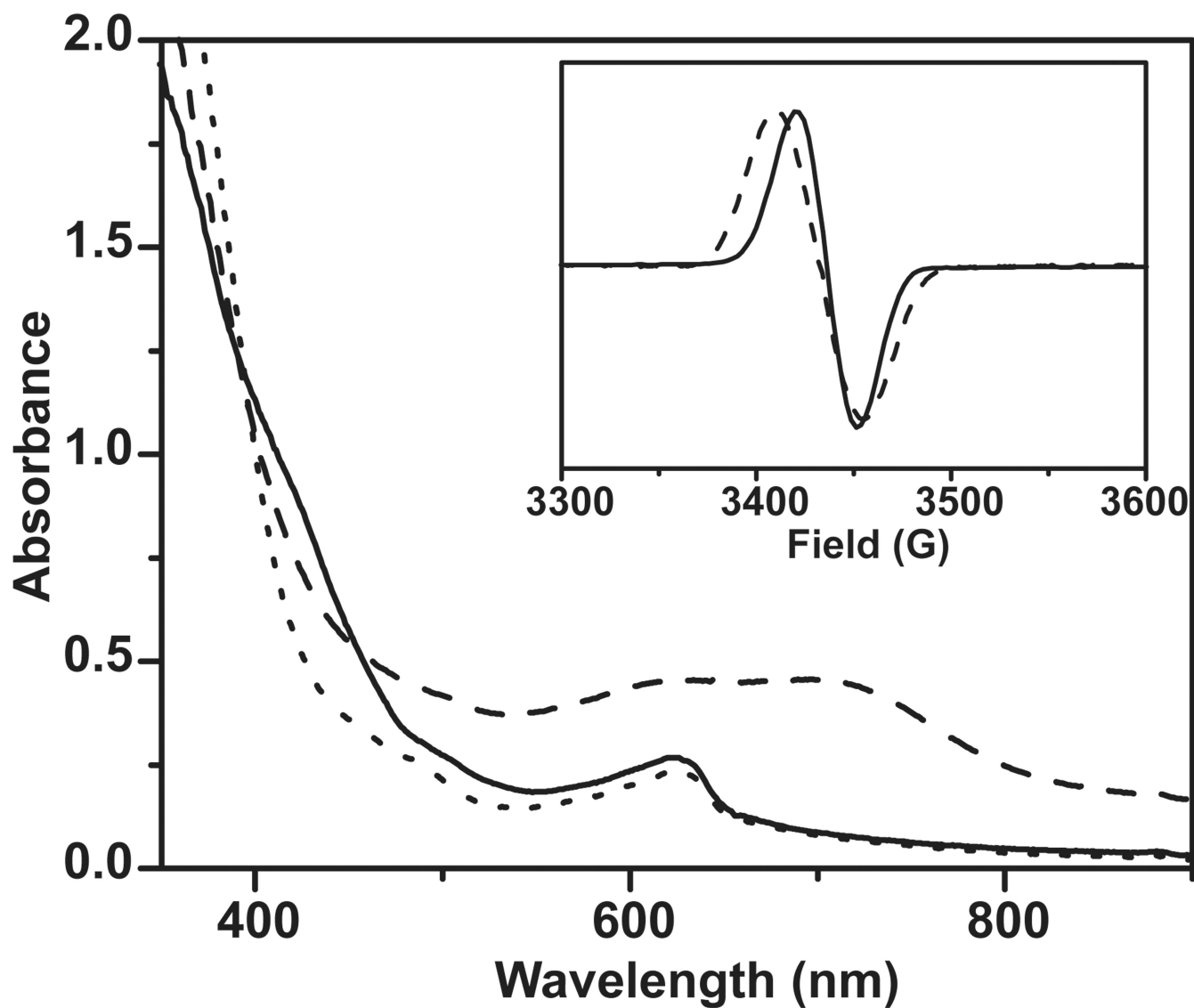
Figure 2.
Reduction of **3** to **4**. Changes observed in the UV-vis spectrum of 0.18 mM **3** (dashed line) upon treatment with 1 equivalent ferrocene at −80 °C to form **4** (solid line) in 3:1 CH_2Cl_2-MeCN. The absorption feature near 450 nm is attributed to **4**, while the one at 620 nm is attributed to ferrocenium ion. The dotted line represents the spectrum of the solution after 2 hours at −80 °C, during which period **4** underwent decay. Inset: EPR spectra of **4** with natural-abundance Fe (solid line) or 95% ^{57}Fe (dashed line) in 3:1 PrCN-MeCN.
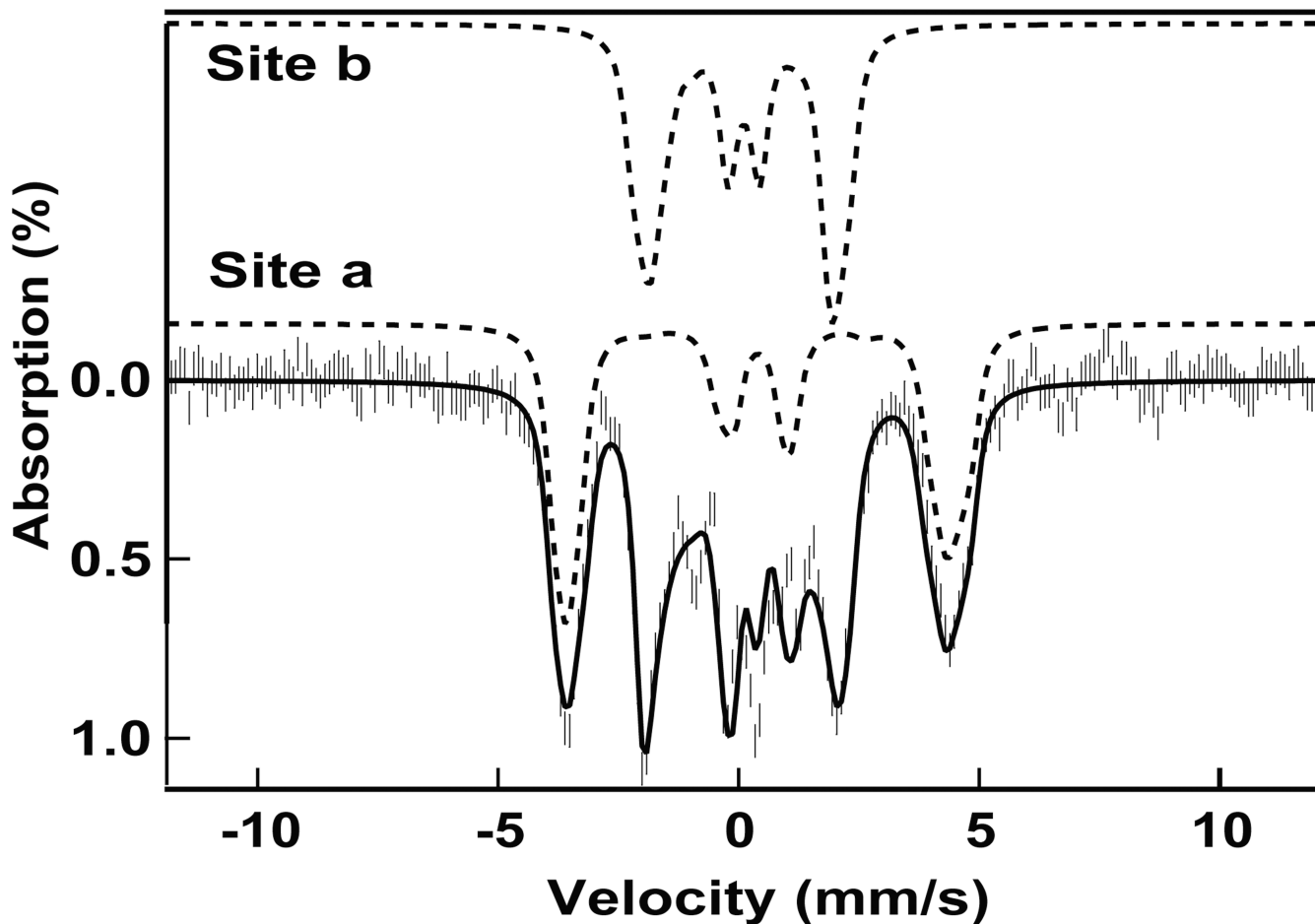
Figure 3.
Mössbauer spectra of **4**. Mössbauer spectrum of **4** obtained in 3:1 PrCN/MeCN (which forms a glass upon freezing) recorded at 4.2 K in a field of 45 mT applied parallel to the observed γ-radiation. The solid line drawn through the data is a theoretical curve based on an $S = \frac{1}{2}$ spin Hamiltonian for two iron sites. Above the data the contributions of sites **a** and **b** (dashed lines), shich correspond to HS ($S_a = 5/2$) Fe^{III} and HS ($S_b = 2$) Fe^{IV}, are shown separately. The raw data, shown in Fig. S2, contained a 37% diiron(III) and an 11% high-spin iron(III) contaminant, which were subtracted from the data shown above.
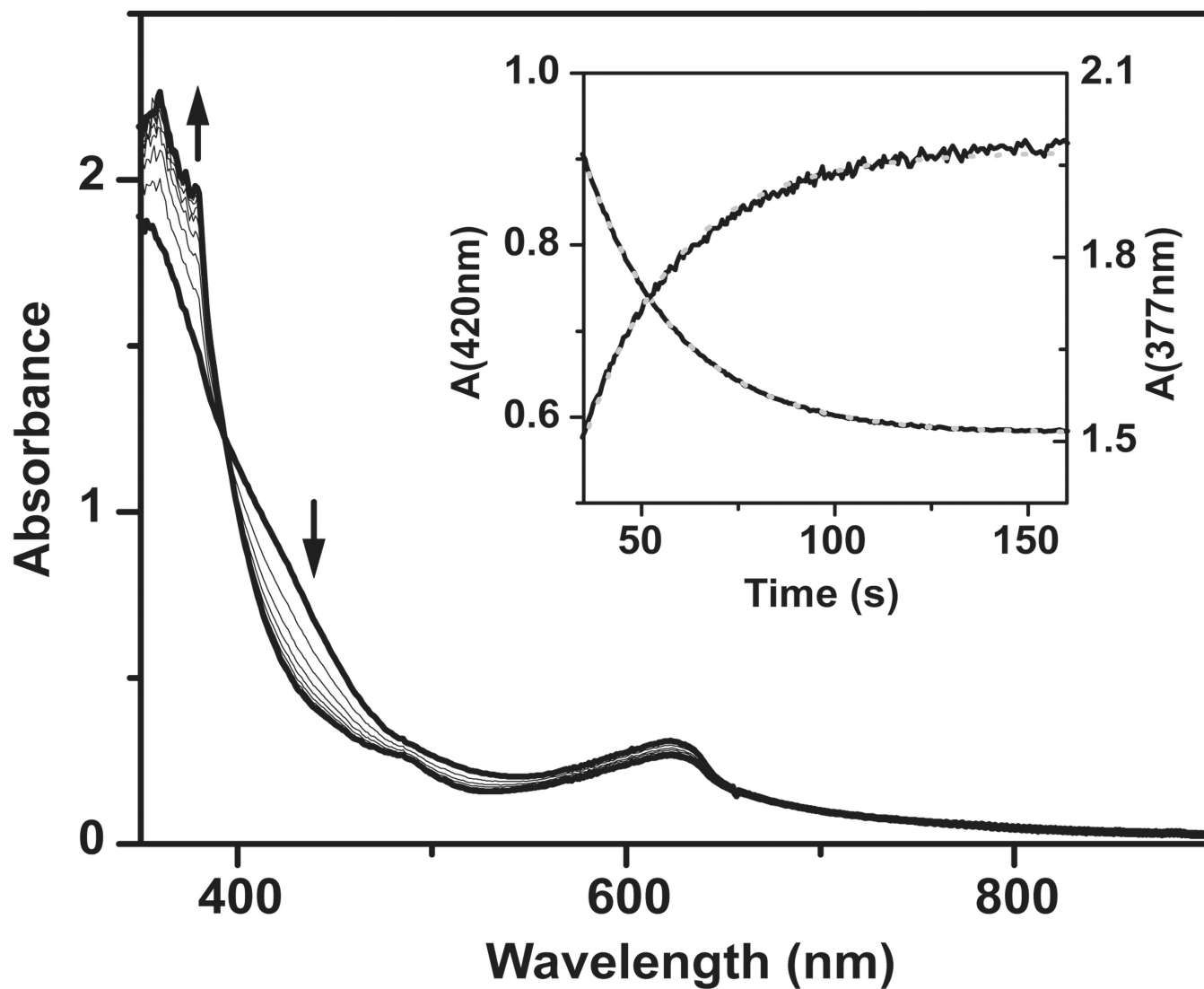
Figure 4.
Reaction of **4** with DHA. UV-vis spectroscopic changes observed upon addition of 1.0 mM DHA to 0.18 mM **4** in 3:1 CH_2Cl_2-MeCN at −80 °C under Ar. Spectra were measured in 10-second intervals. Inset: time traces for the decay of **4** at 420 nm (dashed line) and the formation of the anthracene product at 377 nm (solid line). Both time traces were fit to the same pseudo-first-order model with the same k_{obs}.
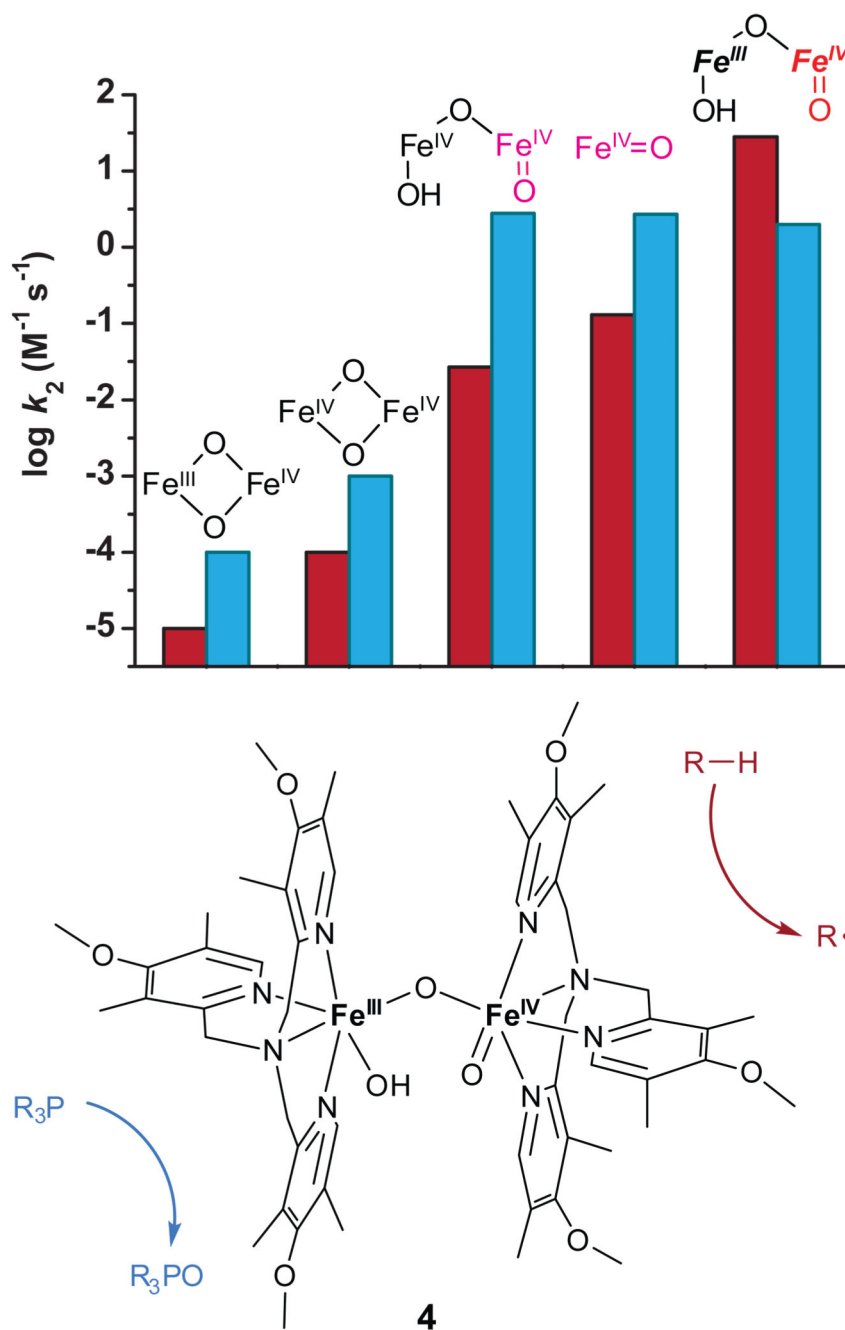
Figure 5.
Graphic comparison of oxidative reactivities of various iron(IV) complexes. (a) From left to right are data for complexes **1**, **2**, **3**, $[Fe^{IV}O(L)(NCMe)]^{2+}$ and **4**. Deep-red bars represent C–H bond cleavage rates (DHA as substrate), while light-blue bars correspond to oxo-transfer rates (diphenyl(pentafluorophenyl)phosphine as substrate). Second order rate constants are listed in Table 1. (b) The structure of **4** and the schematic representation of C–H bond cleavage and oxo-transfer reactions.

Table 1

Comparison of C–H bond cleavage and oxo-transfer reactivities of high-valent iron complexes.

Complex	iron spin state	E_r (mV, vs. $Fc^{+/0}$)[a]	C–H bond cleavage[b]			Oxo-transfer[b]	
			k_2 (M^{-1} s^{-1})	D-KIE[c]	Yield (%)[d]	k_2 (M^{-1} s^{-1})	Yield (%)[d]
1	LS	$270 < E < 490$	10^{-5}	9	ND	10^{-4}	ND
2	LS	760	10^{-4}	10	ND	10^{-3}	ND
3	LS	$490 < E < 670$	0.027	30	80	2.8	99
$[Fe^{IV}O(L)$-$(NCMe)]^{2+}$	LS	$490 < E < 670$	0.13	27	55	2.7	70
4	HS	$490 < E < 670$	28	50	44	2.0	65

[a] Measured by cyclic voltammetry (for **2**) or estimated by potential titration with a reported procedure 16. 10 equivalents of 2,6-lutidinium perchlorate were added to the reactions of **4** with reductants.

[b] DHA and diphenyl(pentafluorophenyl)phosphine were respectively used as the substrates for C–H bond cleavage and oxo-transfer reactions. All k_2 were measured at −80 °C in 3:1 CH_2Cl_2-MeCN under Ar.

[c] The D-KIE value for **4** was determined at −80 °C in 3:1 CH_2Cl_2-MeCN. Values for the other complexes were obtained at −30 °C in MeCN as their rates of DHA-d_4 oxidation were too slow at −80 °C, and those for **1**, **2** and $[Fe^{IV}(O)(L)(NCMe)]^{2+}$ were reported in ref. 16.

[d] The products for C–H bond cleavage and oxo-transfer reactions were anthracene and diphenyl(pentafluorophenyl)phosphine oxide, respectively. ND: not determined due to the slowness of the reactions at −80 °C.